Optical Engineering

OpticalEngineering.SPIEDigitalLibrary.org

Unmanned aerial vehicle-based monitoring of groundwater inputs to surface waters using an economical thermal infrared camera

Charles Abolt
Todd Caldwell
Brad Wolaver
Henry Pai

Charles Abolt, Todd Caldwell, Brad Wolaver, Henry Pai, "Unmanned aerial vehicle-based monitoring of groundwater inputs to surface waters using an economical thermal infrared camera," *Opt. Eng.* **57**(5), 053113 (2018), doi: 10.1117/1.OE.57.5.053113.

Optical Engineering 57(5), 053113 (May 2018)

Unmanned aerial vehicle-based monitoring of groundwater inputs to surface waters using an economical thermal infrared camera

Charles Abolt,[a,b,*] Todd Caldwell,[b] Brad Wolaver,[b] and Henry Pai[c,†]
[a]University of Texas at Austin, Department of Geological Sciences, Austin, Texas, United States
[b]University of Texas at Austin, Bureau of Economic Geology, Austin, Texas, United States
[c]University of Nevada Reno, Department of Geological Sciences and Engineering, Reno, Nevada, United States

Abstract. Groundwater discharge into streams helps maintain flows during droughts and provides refugia for thermally sensitive species, as the relatively constant temperature of spring water buffers against instream diurnal and seasonal fluctuations. Unmanned aerial vehicle (UAV)-based thermal imagery represents an attractive option to monitor sites of groundwater-surface water mixing. However, the use of economical thermal sensors presents several challenges to obtaining a stable dataset for mosaicking. Here, we present a method for acquiring and postprocessing thermal infrared imagery at spring discharge sites using an inexpensive, uncooled microbolometer mounted on a small UAV. The procedure involves initial estimation and removal of pixel bias from the sensor output, and then compensation for temporal sensor drift by optimizing the stability of the signal at ground features detected within multiple frames. We illustrate this approach by presenting a case study at the Devils River, a groundwater dependent stream in Texas. Comparison with imagery acquired using a more expensive thermal camera system, designed to compensate for sensor drift at the time of data acquisition using knowledge of internal camera temperature, reveals that our method produces a more consistent final mosaic image. A good linear fit ($r^2 = 0.97$) between the signal in the stabilized dataset and ground-based measurements of water temperature underscores the potential for this method to inexpensively produce high quality maps of surface temperature in ecologically important stream reaches. [DOI: 10.1117/1.OE.57.5.053113]

Keywords: thermal imaging; uncooled; microbolometer; unmanned aerial vehicles; hydrology.

Paper 180292 received Feb. 23, 2018; accepted for publication Apr. 27, 2018; published online May 24, 2018.

1 Introduction

Water temperature is an important variable in aquatic ecosystems which directly controls the habitat extents of thermally sensitive species. In freshwater streams, water temperature oscillates on annual and daily cycles which are driven by meteorological conditions and influenced by flow volumes.[1] Because the temperature of groundwater usually fluctuates far less than surface water in the same area, groundwater seeps (i.e., springs) have the potential to create relatively stable refugia for riverine species with narrow thermal ranges. These refugia are often warmer than the main surface flow in winter and cooler during the summer, hosting populations of fish, invertebrates, or plants which depend on the spring flow through part of or all the year.[1,2]

One approach to mapping thermal refugia associated with groundwater discharge is to use thermal infrared (TIR) imagery. The pixels of a TIR image indicate the radiance of a surface in the 8 to 14 μm range, which is a function of its temperature and emissivity. Because the emissivity of water is nearly constant, TIR imagery has proven to be a useful tool for inferring stream temperatures from a variety of platforms, ranging from handheld cameras[3] to satellites.[4] Although TIR imagery is sensitive only to temperature in the "skin," or top ~100 μm, of the water column, it can reveal useful information regarding the relative size and extent of groundwater plumes originating from springs on or near the streambank, particularly during winter, when groundwater is most likely to be relatively warm and buoyant.[5]

Unmanned aerial vehicles (UAVs) have become increasingly popular in recent years and represent a promising and cost-effective means of collecting TIR imagery over intermediate scale stream reaches of several hundred meters to several kilometers. However, due to weight limitations, UAVs tend to be mounted with small, uncooled thermal cameras. The output of these sensors is influenced considerably by variation in camera temperature, which tends to be highly unstable during a flight.[6] In some applications of thermal imaging, such as fire mapping,[7] estimation of thermal loading around buildings,[8] or search and rescue operations,[9] the resulting sensor drift may be small compared to differences in thermal intensity between the target and the background, which are associated with temperature differences of several tens of degrees Celsius. However, applying effective corrections for sensor drift is far more important at sites of groundwater-surface water mixing, where key temperature differences often are only several degrees.[10] To date, only a handful of studies have yet employed UAV platforms to collect TIR imagery over any stream environments,[11–13]

*Address all correspondence to: Charles Abolt, E-mail: chuck.abolt@beg.utexas.edu

†Present address: Northwest River Forecast Center, National Oceanic and Atmospheric Administration, Portland, Oregon

0091-3286/2018/$25.00 © 2018 SPIE

necessitating the development of new methods to produce data with sufficient thermal precision.

In this paper, we present a postprocessing method to stabilize imagery from the Forward Looking Infrared Systems (FLIR, Wilsonville, Oregon, United States) Vue Pro, an economically priced uncooled microbolometer weighing approximately 100 g. We apply the method in a case study at the Devils River in Val Verde County, Texas. We produce a mosaic from 230 postprocessed still frame images and compare it with the unprocessed imagery and with ground-based observations of temperature at discrete points. Finally, we compare the stabilized mosaic with another mosaic produced using the FLIR Tau2, a more expensive camera, which uses a proprietary algorithm to stabilize imagery at the time of data acquisition.

2 Background

All microbolometers include a focal plane array of elements sensitive to incident longwave infrared radiation. The equation relating voltage at each array element (or pixel) to the radiant flux from the scene takes a linear form:

$$V_{i,j} = x_{1_{i,j}} R_{i,j} + x_{0_{i,j}}, \tag{1}$$

where the coefficient $x_{1,i,j}$ relates the voltage, V, at pixel (i, j) to the thermal radiance, $R_{i,j}$, originating from that portion of the field of view; and the term $x_{0,i,j}$ represents other factors to which the voltage is sensitive, including thermal radiation originating from the camera interior.[14] Whenever data is collected, the camera effectively rearranges Eq. (1) to convert voltage to a signal, S, in units of "counts," or digital numbers proportional to scene-based radiance:

$$S_{i,j} = o_{1_{i,j}} V_{i,j} + o_{0_{i,j}}. \tag{2}$$

For this procedure to work, the camera must have knowledge of the correct offset compensation coefficients, o, which are stored in internal memory.

In all longwave infrared cameras, the values of o vary from pixel to pixel, and therefore must be calibrated prior to data acquisition. In uncooled microbolometers, such as the Vue Pro we used, an extra layer of complexity is introduced, as the correct values of o also vary as a function of the camera's internal temperature. Because the internal temperature of the camera changes substantially during a UAV flight, the coefficients for each pixel drift over time, each at a different rate. Therefore, to maintain the integrity of the imagery, it is necessary for the camera to periodically update its calibration. Many uncooled systems do so through execution of a nonuniformity correction (NUC) procedure, during which the internal shutter, assumed to be a uniform temperature source, is presented to the focal array, and the camera's estimates of o are adjusted such that each pixel records the same radiant flux. This procedure is intended to assure that, within a single image, the signal at each pixel is proportional to the scene-based radiance. However, the procedure does not ensure that the linear relationship between signal and radiant flux remains constant among multiple images, particularly when they are separated by one or more instances of the NUC. This effectively means that imagery from a UAV flight is affected by temporal sensor drift, which may distort temperature estimates by several degrees Celsius over the course of a flight and must be removed prior to mosaicking.

In addition to temporal drift, one other form of data instability that can compromise the quality of a mosaic image is fixed-point noise, or pixel bias. This bias distorts individual still frames and is attributed in large part to longwave radiation reflected off the inside of the camera lens toward the sensor array, which is not visible when the internal shutter is closed.[15,16] The bias therefore persists through application of a shutter-based NUC, producing a vignetting-like effect, in which the edges of an image appear darker than the center. Like temporal drift, this effect may represent the equivalent of several degrees Celsius on sensor output. The magnitude and spatial pattern of pixel bias may change over the course of a UAV flight, but within individual frames, it tends to vary smoothly from pixel to pixel.

Because the digital signal output by a microbolometer is proportional to radiant flux, an appropriate conversion must be made to derive surface temperature, once data have been stabilized. The equation relating digital signal to temperature takes the form:

$$S(T) = \frac{R}{\exp(B/T) - F} + O, \tag{3}$$

where T is the temperature in kelvin, and the fitting parameters R, B, F, and O must be calibrated to the sensor.[17] Although Eq. (3) is used in practice to interpret the signal from sensors designed to monitor broad temperature ranges, the relationship tends to be nearly linear when constrained to ambient temperatures commonly observed at Earth's surface.

3 Equipment

3.1 *FLIR Vue Pro*

The camera on which we focused our study was the FLIR Vue Pro, an uncooled microbolometer that retails for approximately \$2000. The camera has a 9-mm Germanium lens with a 69 deg × 56 deg field of view, and a sensor array of 640 × 512 elements, sensitive to the spectral band from 7.5 to 13.5 μm. The FLIR Vue Pro requires a 5V external power source and records still frame or video imagery directly onto a micro SD card inserted into its side. It includes a built in GoPro-style mount, which we used for attachment to the front of our UAV in a nadir-viewing position. The camera features a shutter-based NUC procedure, but it does not have any means of correcting for temporal drift caused by instability in internal temperature.

3.2 *FLIR Tau2*

The second camera used in this study was the FLIR Tau2, another uncooled microbolometer, which has similar optical specifications to the Vue Pro and retails for approximately \$10,000. The Tau2 also requires an external 5V power source, but unlike the Vue Pro, it requires an external system to store digital output, provided by ICI (Infrared Cameras Inc., Beaumont, Texas, United States). The key innovation of the Tau2 beyond the Vue Pro is that it includes a thermistor to monitor internal camera temperature while data is collected. The coefficients o from Eq. (2) are calibrated in the factory as a function of internal temperature to stabilize the digital signal as temperature varies. Because the camera is designed to remove temporal sensor drift at the time of data acquisition, it can be paired with ICI IR Flash software to output digital images in which the signal has already been converted to absolute temperature.

4 Study Site and Data Acquisition

The study site was centered on Finegan Springs (∼29.900°N, 100.998°E), a large karst spring on the banks of the Devils River[18] in the Edwards Plateau region of Texas (Fig. 1). Originating on the east bank of the stream, Finegan Springs flows persistently throughout the year and provides aquatic habitats for the federally threatened Devils River minnow (*Dionda diaboli*),[18,20] the federally endangered Texas Hornshell mussel (*Popenaias popeii*),[21,22] and other aquatic species of conservation interest.[2] At the mouth of the spring, the river is ∼30 m wide and flows through an incised bedrock channel. During the week of data collection, we measured streamflow (using a FlowTracker acoustic Doppler velocimeter, SonTek, San Diego, California, United States) of $\sim 1.16\ \mathrm{m^3\,s^{-1}}$ approximately 1 km upstream from the spring.

Data collection with the FLIR Vue Pro began at 9:57 AM on February 9, 2017, approximately two and a half hours after sunrise. The sky was free of clouds and air temperature was 15.6°C with 44% relative humidity. We programmed our UAV to fly along the stream at an altitude of 65 m from ∼300 m downstream of the main spring outlet to 200 m upstream; it first flew up the east bank, then down the middle of the channel, and up the west bank at a velocity of $5\ \mathrm{m\,s^{-1}}$. Still frame images were collected once per second, and a NUC was programmatically triggered every 5 s.

During the flight, we monitored temperature at three water baths located along the eastern bank of the stream, using TidbiT temperature sensors (manufacturer accuracy ±0.2°C; Onset Computer Corporation, Bourne, Massachusetts, United States) programmed to record every minute. The water baths were created in plastic pools, approximately 1 m in diameter and a quarter meter deep. Each water bath was filled with different ratios of spring to stream water to produce a wide range of temperatures. Additionally, we monitored water temperature at the mouth of Finegan Springs using the same sensor, to acquire ground-based temperature observations at a total of four points. Observations at these points were subsequently compared with the UAV imagery to develop a curve relating the camera signal to surface temperature.

Approximately an hour and a half following the flight of the FLIR Vue Pro, imagery from the site was captured using the FLIR Tau2 from an altitude of 80 m. The flight path overlapped most of the area surveyed with the FLIR Vue Pro but was offset slightly upstream. The ICI IR-flash software was used to process images from the Tau2 and derive surface temperature, measured in °C. Therefore, no image stabilization procedure was later applied to data from the Tau2. Imagery from the second flight was processed into a mosaic image and compared with data from the FLIR Vue Pro.

5 Image Stabilization Procedure

Our workflow for stabilizing the FLIR Vue Pro imagery involved two corrections to each frame (Fig. 2). The first correction was designed to compensate for pixel bias within

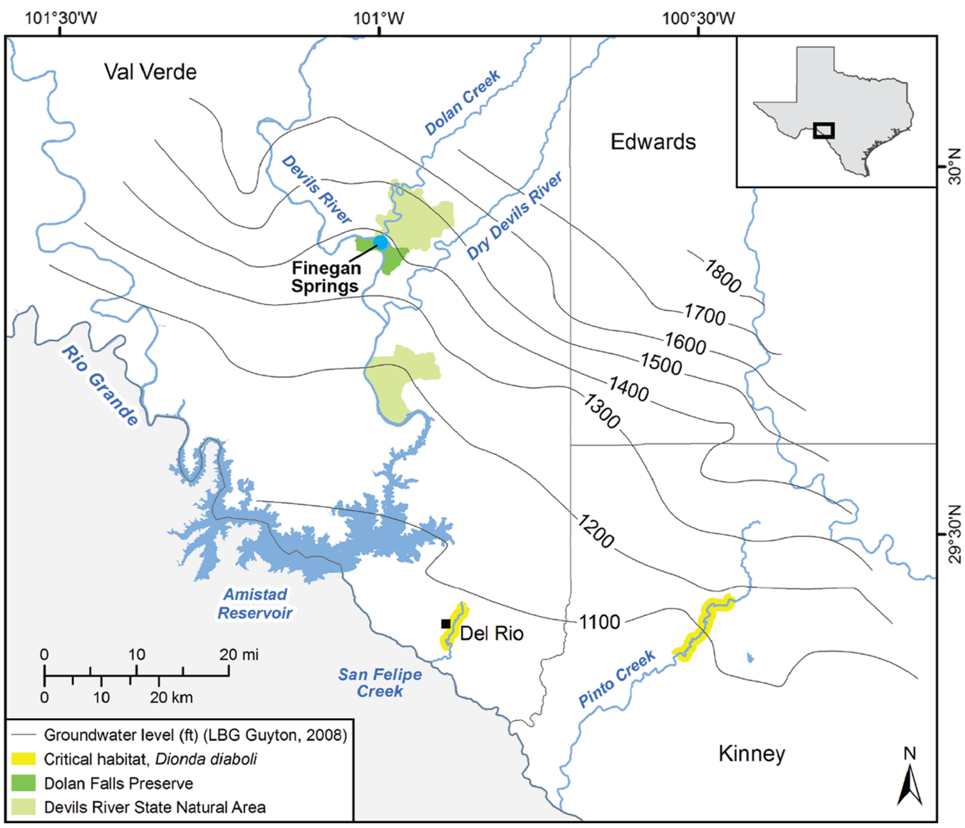

Fig. 1 Location of study area on the Devils River within Dolan Falls Preserve, including critical habitat for *Dionda diaboli*.[19]

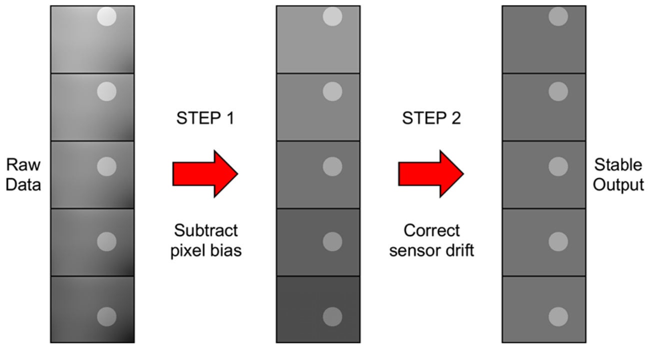

Fig. 2 Flowchart of our two-step procedure for stabilizing the raw output of the FLIR Vue Pro. The gray circle denotes a ground feature within a stack of raw images. The feature and the background are depicted at uniform but different temperatures. In the first step, pixel bias, or distortion within individual frames, is removed. In the second step, sensor drift is corrected using an optimized linear adjustment to each frame. Image intensity in the stable output is eventually converted to surface temperature through calibration against a set of ground measurements.

individual images. The second correction was a linear intensity adjustment unique to each image, designed to counteract temporal drift by optimizing the stability of the signal at features observed across multiple frames.

We were motivated to develop this workflow due to a lack of pre-existing methods that: (1) are designed to stabilize datasets affected by both pixel bias and temporal drift and (2) are practicable using the hardware incorporated into the Vue Pro. A number of prior methods have been developed which, like the algorithm used by Tau2, involve performing a calibration to remove sensor drift and pixel bias as a function of internal temperature.[23,24] However, these methods are inapplicable to the Vue Pro, due to the lack of internal thermistors. Several methods that do not require additional hardware have been developed to remove pixel bias.[15,16,25] However, some rely on an assumption of negligible sensor drift[25] (inapplicable in our case), and the remainder do not address the problem of sensor drift at all. To our knowledge, our method is the first presented that is capable of removing significant distortion attributed to both pixel bias and sensor drift in the Vue Pro or any other uncooled microbolometer with a shutter-based NUC procedure.

Conceptually, applying the first step of our procedure involved estimating and then subtracting the pixel bias from each frame. We reviewed previously developed approaches to this objective and tested one popular method designed to estimate the unique bias in each frame by isolating spatially continuous, low gradient variation in image intensity from high gradient variation associated with the scene.[15] We found that this method effectively removed pixel bias from some of our images, but performed poorly on others, as spatial variation in water temperature often was mistakenly identified as noise (Fig. 3). Through experience with the camera, we determined that a suitable method for estimating pixel bias in the FLIR Vue Pro was by imaging the lens cap just after landing and assuming it to be a uniform temperature source. Although this approach neglects temporal variation in pixel bias, we found that by allowing the camera to warm up for roughly an hour before data acquisition and by frequently applying the shutter-based NUC, the temporal variation is significantly reduced. By computing the mean of fifteen images of the lens cap immediately following landing, we estimated that the most positively

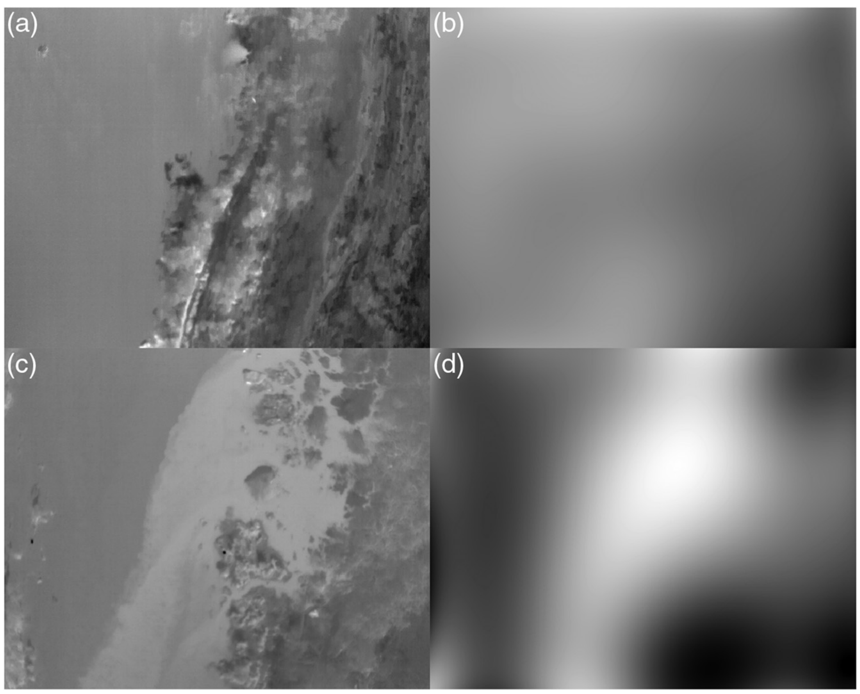

Fig. 3 Results from the application of a popular method for removing pixel bias[15] to our dataset, including (a) an image at the start of our flightpath and (b) estimated pixel bias; and (c) an image at the main seep of Finegan Springs and (d) estimated pixel bias. Note similarity between panel (b) and Fig. 4, implying success. In contrast, results in panel (d) clearly demonstrate that the method mistakes some variation in water temperature for pixel bias. Estimated pixel bias in panels (b) and (d) is normalized between 0 and 160 photon counts.

biased pixels in our flight over the springs were ~130 digital counts brighter than the most negatively biased pixels (Fig. 4). This bias was subtracted from each image in the dataset.

The second correction was a linear adjustment to the intensity of each frame. This correction was intended to correct for sensor drift driven by temporal variation in the internal temperature of the camera. In making this adjustment, we relied on the assumption that signal in each image (after the subtraction of estimated pixel bias) was proportional to scene-based radiance, but that the ratio of signal to radiant flux was inconsistent among images. Therefore, we sought a pair of linear coefficients for each frame, to stabilize the signal throughout the dataset. Our approach to estimating these coefficients was to trace time variation in the signal at a large set of ground points, each detectable in multiple frames, and then identify the set of corrections that minimized signal variation at each ground point.

We identified ground points using Agisoft Photoscan, a popular commercial software package that uses proprietary algorithms to track the movement of features across a camera's field of view with subpixel precision. For illustration, Fig. 5 shows a set of 30 randomly selected ground points identifiable in a pair of images collected three seconds apart, while the UAV flew near one of the larger seeps of Finegan Springs. Overall, from our set of 230 images, Agisoft Photoscan identified 68,417 discrete ground points; on average, more than 1200 were detectable in each frame of imagery. At every instance of a detected ground point in our dataset, we extracted the mean signal intensity within a ten-pixel radius.

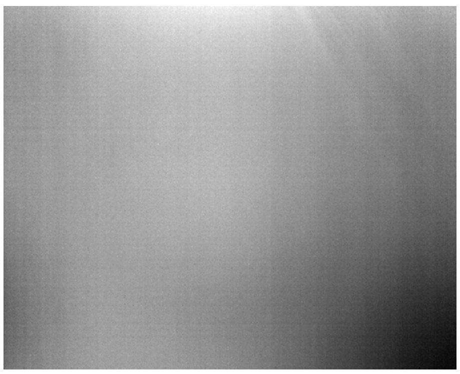

Fig. 4 Average of 15 images of the lens cap captured by the FLIR Vue Pro immediately following landing, used to infer pixel bias. The most positively biased pixels were 130 photon counts brighter than the most negatively biased pixels. This image was subtracted from all still frames in the first step of our stabilization procedure.

We then applied a global optimization routine, the shuffled complex evolution algorithm developed at the University of Arizona (SCE-UA), to identify the optimal set of linear coefficients to apply to the frames. SCE-UA is a popular genetic algorithm in which a collection of simplexes, or sets of trial solutions, evolve simultaneously, exchanging information with one another while exploring a predefined parameter space to minimize an objective function.[26] SCE-UA handles high-dimensional problems (i.e., those with many parameters), especially well, and has been very successful in the past as a tool for calibrating complex hydrologic models.[27–29] We used the algorithm to optimize the coefficients, x, for each frame, such that:

$$I'_{i,j} = x_1 I_{i,j} + x_o, \tag{4}$$

where I is the intensity of the pixel at coordinates (i, j) before the correction and I' is the intensity postcorrection. The objective function was computed by calculating a weighted mean of the standard deviation of the adjusted signal at selected ground points, in which the assigned weight was proportional to the number of frames in which that point was detected. To increase computational efficiency, the objective function incorporated only a subset of the ground points identified in Agisoft Photoscan, chosen such that each frame contained at least thirty instances. We generally allowed x_1 for each frame to vary between 0.9 and 1.1, and x_0 to vary between −40 and +40. These bounds were set to be arbitrarily large; in practice, we found that the parameters nearly always calibrated within the inner 25% of the defined limits. To prevent artificial reduction of the signal in the optimized dataset, in the first frame, x_1 was not allowed to decrease below 1.0, and x_0 was not allowed to be negative.

To illustrate this approach, Figs. 4 and 6 show sample results obtained by applying it to a subset of 15 images near the start of the flight path. Thirty ground control points, each represented by a colored "x," were selected at random. In this example, the weighted mean of the standard deviation in signal intensity at each point decreased from 14.4 to 3.2 digital counts.

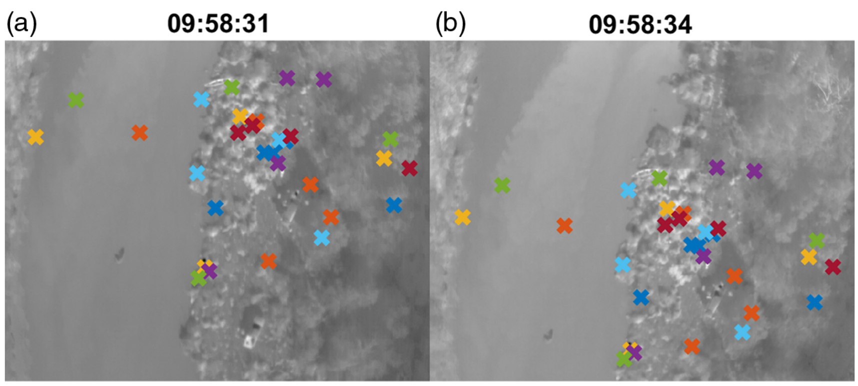

Fig. 5 (a) and (b) A pair of images captured 3 s apart, with 30 shared ground points marked.

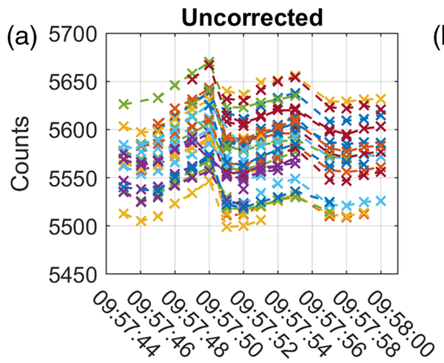

Fig. 6 Illustration of the stabilization of signal intensity in 15 images using our approach. Each line represents the signal at a ground feature detectable across multiple frames, shown (a) before and (b) after postprocessing.

Although SCE-UA is well suited to optimize large sets of parameters simultaneously, computation time increases nonlinearly as the number of parameters increases. Therefore, to accelerate the procedure, we implemented the algorithm in two phases, taking advantage of the linear nature of the solution. In the first phase, the 230 images were stabilized in groups of roughly 15. The groups were assigned based on the geographic position of the still frame from downstream to upstream, which was stored in a text file generated by Agisoft Photoscan; therefore, each group included

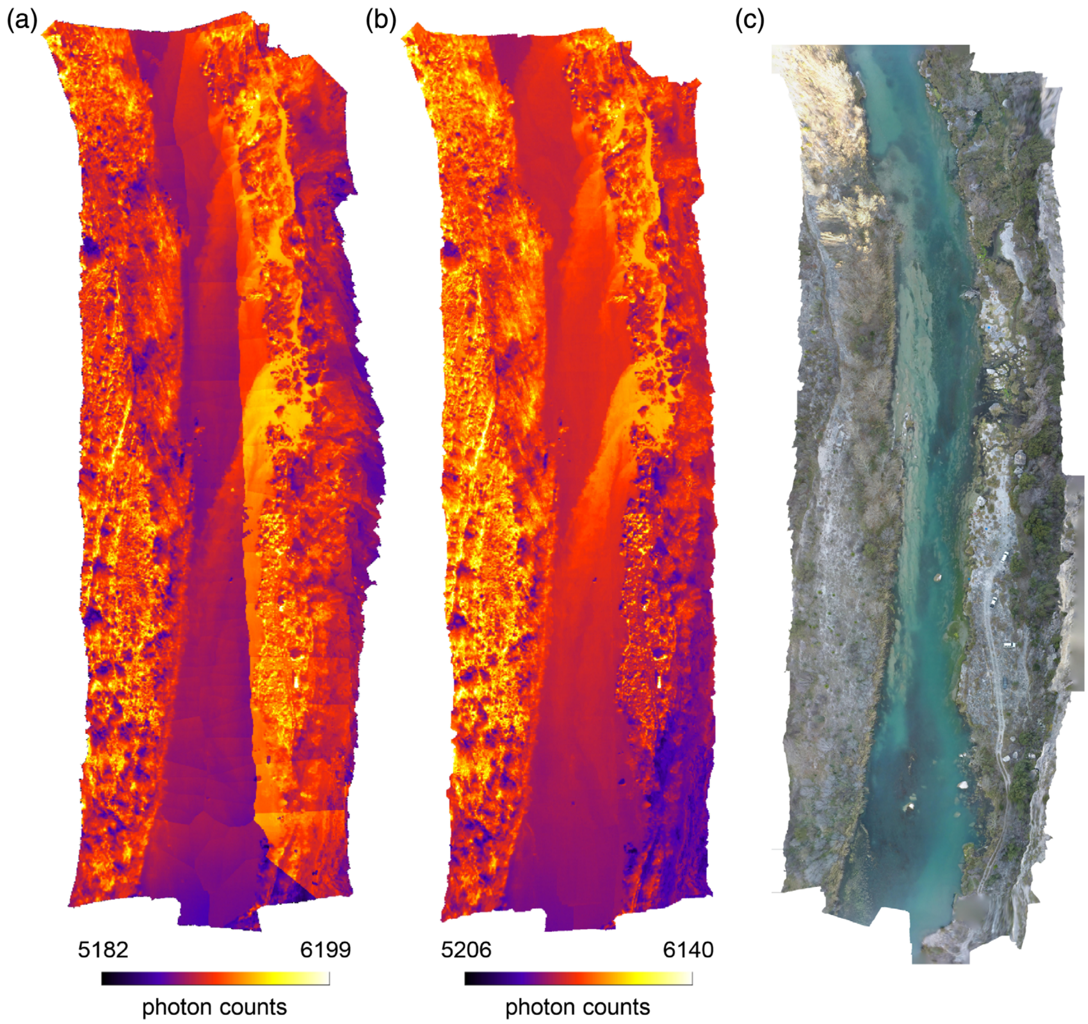

Fig. 7 Mosaic of imagery from the FLIR Vue Pro (a) before postprocessing and (b) after postprocessing, with (c) visual imagery provided for reference. Note trucks in lower-right quadrant of imagery for scale.

images from all three legs of the flight path. In the second phase, an additional set of coefficients was optimized for each group, to stabilize the entire dataset. Run on a personal laptop, the optimization procedure was completed in less than 8 min.

6 Results

Mosaic images are presented in Fig. 7 constructed using uncorrected output from the FLIR Vue Pro (a) and imagery that has been postprocessed using our method (b). The mosaic images were produced in Agisoft Photoscan with blending options disabled. The intensity of any pixel in the mosaics is therefore derived solely from the image in which the camera is pointed most nearly perpendicular to the ground at that point. Our method of postprocessing considerably reduces the sensor drift evident in the unprocessed mosaic; although the major spring discharge is notable in both images midway down the eastern bank, the instability among frames is much more pronounced in the unprocessed imagery. Upon application of our method, the weighted mean of the standard deviation of the signal at the ground points used for data stabilization dropped from 37.6 digital counts in the original to 4.4. The corrected image presents a sharp representation of several groundwater seeps entering the east bank of the river. At each seep, the warmer and more buoyant groundwater enters the surface flow at the top of the water column, gradually mixing with the cooler, underlying river water as it flows downstream.

A mosaic constructed from imagery acquired by the FLIR Tau2 is shown in Fig. 8. The spatial extent of the figure overlaps the mosaics in Fig. 7 but depicts the study area approximately an hour later in the day. Figure 8 was also constructed with blending options disabled in Agisoft Photoscan. As indicated by the color bar, the imagery has units of temperature, rather than digital counts. It is evident that, despite the internal procedures designed to compensate for variation in internal camera temperature, the Tau2 is affected considerably by sensor drift throughout the UAV flight. The discordance between adjacent legs of the flight path implies high levels of uncertainty in the real surface temperature.

Postprocessed imagery from the FLIR Vue Pro aligns well with ground-based water temperature measurements; a linear regression between four ground points and pixel intensity extracted from the postprocessed mosaic reveals a close fit ($r^2 = 0.97$) with a slope of approximately 1°C/18 digital counts (Fig. 9). The close match between camera signal and water temperature underscores the potential to produce maps of surface temperature by applying our method of data stabilization to the output of the FLIR Vue Pro. Comparison of surface temperature at 200 randomly selected points from the river, estimated both through our method and from the Tau2 imagery, reveals that the Tau2 predicts temperatures generally cooler than the Vue Pro; at times, the difference is as much as 3°C (Fig. 10).

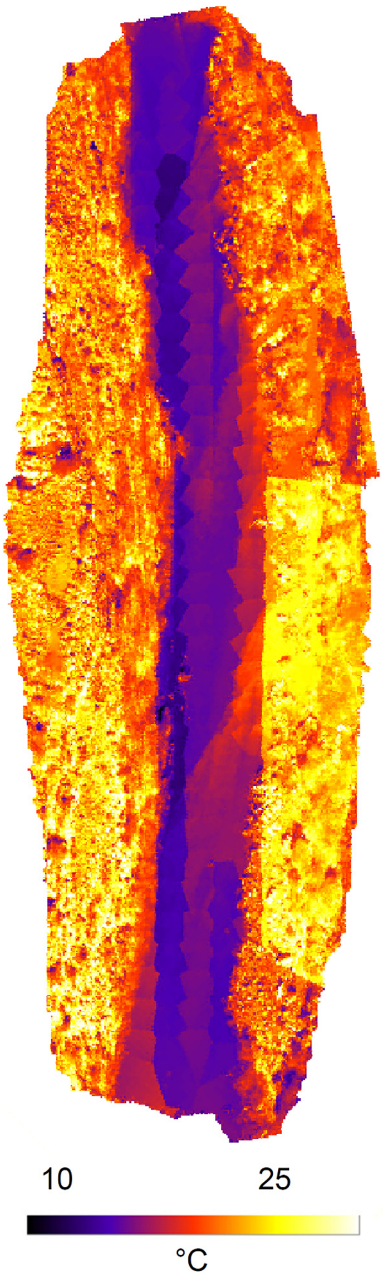

Fig. 8 Mosaic of imagery from the FLIR Tau2.

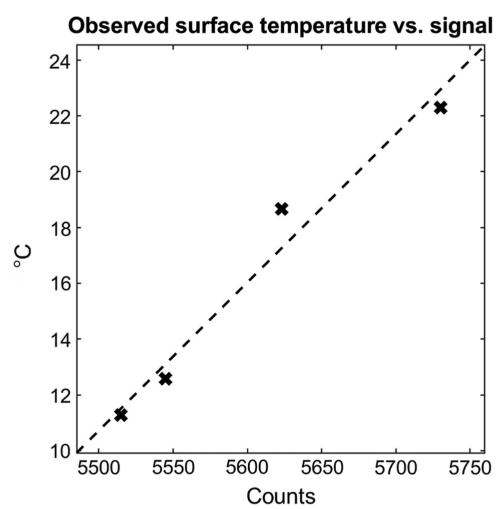

Fig. 9 Comparison of signal from postprocessed FLIR Vue Pro imagery with water temperature measured on the ground.

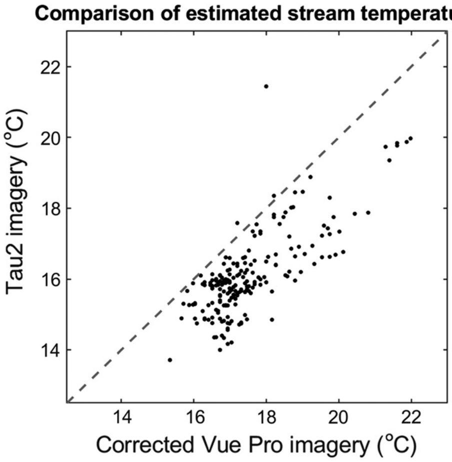

Fig. 10 Comparison of estimated river temperature at 200 points, using our method applied to Vue Pro imagery and Tau2 imagery.

7 Conclusions

Despite the challenges of compensating for data instability, the collection of longwave infrared imagery from a UAV platform is a promising method for mapping surface water temperatures associated with groundwater-surface water mixing. By applying a postprocessing procedure designed to stabilize the intensity of ground features detected frequently during a flight, we assembled data from an inexpensive thermal camera into a stable mosaic of thermal radiance along a ~500-m stretch of river affected by several groundwater seeps. The advantages of our postprocessing method are that it performs well on data from an economical sensor (~2,000 for the Vue Pro we used) and produces a smoother mosaic image than data from a more expensive system (~10,000 for the Tau2 with accessories). The main disadvantage is that the imagery produced through our method must be converted to surface temperature through calibration against a set of ground measurements. Nonetheless, strong alignment between the signal in the postprocessed imagery and observed water temperature at our field site implies that the method can be used effectively to estimate near-surface stream temperatures, and thereby monitor the habitat of thermally sensitive species.

Acknowledgments

Support for this project was provided in part by the U.S. Fish and Wildlife Service and Texas Parks and Wildlife Department (Grant #TX E-173-R-1, F15AP00669 to BW and TC), the Jackson School of Geosciences through a seed grant awarded to BW and TC, the NASA Earth and Space Science Fellowship program through an award to CA, and the Center for Transformative Environmental Monitoring Programs (CTEMPS) funded by the National Science Foundation. We thank S. Robertson, J. Joplin, B. Hester, W. Collins, K. Mayes, S. Magnelia, B. Birdsong (TPWD) for financial and logistical support at the Devils River State Natural Area; S. Tyler, S. Sladek, and C. Kratt (CTEMPS) for acquiring FLIR Tau2 data and piloting UAV; J. Pierre, J. Andrews, and C. Breton (UT-Austin) for help with field data collection and mapping; M. Montagne, P. Diaz, and R. Gibson (USFWS) for support; and R. Smith and D. Meyer at The Nature Conservancy for providing access and lodging at the Dolan Falls Preserve.

Data and code availability: Imagery and code are available at https://github.com/chuckaustin/devilsRiver.

References

1. R. N. Handcock et al., "Thermal infrared remote sensing of water temperature in riverine landscapes," in *Fluvial Remote Sensing for Science and Management*, John Wiley & Sons, Hoboken, New Jersey (2012).
2. K. A. Kollaus and T. H. Bonner, "Habitat associations of a semi-arid fish community in a karst spring-fed stream," *J. Arid Environ.* **76**, 72–79 (2012).
3. M. B. Cardenas et al., "Ground-based thermography of fluvial systems at low and high discharge reveals complex thermal heterogeneity driven by flow variation and bioroughness," *Hydrol. Processes* **22**, 980–986 (2008).
4. E. Lalot et al., "Quantification of the contribution of the Beauce groundwater aquifer to the discharge of the Loire River using thermal infrared satellite imaging," *Hydrol. Earth Syst. Sci.* **19**, 4479–4492 (2015).
5. D. K. Hare et al., "A comparison of thermal infrared to fiber-optic distributed temperature sensing for evaluation of groundwater discharge to surface water," *J. Hydrol.* **530**, 153–166 (2015).
6. A. M. Jensen and Y. Chen, "Procedures for processing thermal images using low-cost microbolometer cameras for small unmanned aerial systems," in *Proc. of the Geoscience and Remote Sensing Symp. (IGARSS '14)*, pp. 2629–2632 (2014).
7. F. Li et al., "Using high-resolution UAV-borne thermal infrared imagery to detect coal fires in Majiliang mine, Datong coalfield, Northern China," *Remote Sens. Lett.* **9**, 71–80 (2018).
8. N. Gaitani et al., "High-resolution spectral mapping of urban thermal properties with unmanned aerial vehicles," *Build. Environ.* **121**, 215–224 (2017).
9. M. Silvagni et al., "Multipurpose UAV for search and rescue operations in mountain avalanche events," *Geomatics Nat. Hazards Risk* **8**, 18–33 (2017).
10. H. Pai et al., "Potential for small unmanned aircraft systems applications for identifying groundwater-surface water exchange in a meandering river," *Geophys. Res. Lett.* **44**, 11,868–11,877 (2017).
11. S. J. Dugdale, "A practitioner's guide to thermal infrared remote sensing of rivers and streams: recent advances, precautions and considerations," *WIREs Water* **3**, 251–268 (2016).
12. V. Wawrzyniak et al., "Prediction of water temperature heterogeneity of braided rivers using very high resolution thermal infrared (TIR) images," *Int. J. Remote Sens.* **34**, 4812–4831 (2013).
13. A. M. Jensen et al., "Thermal remote sensing with an autonomous unmanned aerial remote sensing platform for surface stream temperatures," in *Proc. of the Geoscience and Remote Sensing Symp. (IGARSS '12)*, pp. 5049–5052 (2012).
14. H. Budzier and G. Gerlach, "Calibration of uncooled thermal infrared cameras," *J. Sens. Sens. Syst.* **4**, 187–197 (2015).
15. Y. Cao and C. L. Tisse, "Single-image-based solution for optics temperature-dependent nonuniformity correction in an uncooled long-wave infrared camera," *Opt. Lett.* **39**, 646–648 (2014).
16. L. Liu and T. Zhang, "Intensity non-uniformity correction of aerothermal images via lp-regularized minimization," *J. Opt. Soc. Am. A* **33**, 2206–2212 (2016)
17. J. M. Lloyd, "Thermal imaging systems," Springer Science+Business Media, New York (1975).
18. R. T. Green, F. P. Bertetti, and M. S. Miller, "Focused groundwater flow in a carbonate aquifer in a semi-arid environment," *J. Hydrol.* **517**, 284–297 (2014).
19. U.S. Fish and Wildlife Service, "Endangered and threatened wildlife and plants; designation of critical habitat for the Devils River Minnow," *Fed. Regist.* **73**, 76988–47026 (2008).
20. U.S. Fish and Wildlife Service, *Devils River Minnow (Dionda Diaboli) Recovery Plan*, U.S. Fish and Wildlife Service, Albuquerque, New Mexico (2005).
21. U.S. Fish and Wildlife Service, "Endangered and threatened wildlife and plants; endangered species status for Texas hornshell," *Fed. Regist.* **83**, 5720–5735 (2018).
22. C. R. Randklev et al., "A semi-arid river in distress: contributing factors and recovery solutions for three imperiled freshwater mussles (family: unionidae) endemic to the Rio Grande basin in North America," *Sci. Total Environ.* **631**, 733–744 (2018).
23. A. Tempelhahn et al., "Improving the shutter-less compensation method for TEC-less microbolometer-based infrared cameras," *Proc. SPIE* **9451**, 94511F (2015).
24. R. Strakowski and B. Wiecek, "Temperature drift compensation in metrological microbolometer camera using multi sensor approach," in *Proc. of the 13th Quantitative Infrared Thermography Conf. (QIRT)*, pp. 791–798 (2016).
25. A. Averbuch, G. Liron, and B. Z. Bobrovsky, "Scene based non-uniformity correction in thermal images using Kalman filter," *Image Vision Comput.* **25**, 833–851 (2007).

26. Q. Y. Duan, S. Sorooshian, and V. Gupta, "Effective and efficient global optimization for conceptual rainfall-runoff models," *Water Resour. Res.* **28**, 1015–1031 (1992).
27. V. A. Cooper, V. T. V. Nguyen, and J. A. Nicell, "Evaluation of global optimization methods for conceptual rainfall-runoff model calibration," *Water Sci. Technol.* **36**, 53–60 (1997).
28. K. Eckhardt and J. G. Arnold, "Automated calibration of a distributed catchment model," *J. Hydrol.* **251**, 103–109 (2001).
29. G. Kan et al., "A heterogeneous computing accelerated SCE-UA global optimization method using OpenMP, OpenCL, CUDA, and OpenACC," *Water Sci. Technol.* **76**, 1640–1651 (2017).

Charles Abolt is a PhD candidate in the Jackson School of Geosciences at the University of Texas at Austin. He has an MS degree in geological sciences from UT Austin and a BA degree from Duke University. His research focuses on numerical modeling and remote sensing of near-surface hydrologic processes and is funded by a NASA Earth and Space Science Fellowship.

Todd Caldwell is a research hydrogeologist and soil scientist with the Bureau of Economic Geology at the University of Texas at Austin. His research focuses on field investigations, remote sensing, and modeling of vadose zone processes across multiple scales and environments. He is principal investigator for the Texas Soil Observation Network, a core validation site for NASA's Soil Moisture Active Passive Satellite Mission.

Brad Wolaver develops science to inform aquatic and terrestrial habitat conservation for federal, state, nonprofit, and private stakeholders. His research at The University of Texas at Austin focuses on ground water-surface water interactions, groundwater-dependent ecosystems, landscape ecology, and US-Mexico transboundary groundwater resource management. He graduated from the UT Austin Jackson School of Geosciences and the University of Arizona Department of Hydrology and Water Resources. He studied aridland hydrology as a Fulbright Scholar in Chile.

Henry Pai is a hydrologist with the National Oceanic and Atmospheric Administration. At the time of this study, he was a postdoctoral scholar at University of Nevada, Reno, and working with the Center for Transformative Environmental Monitoring Programs. He has a BS degree in electrical engineering and an MS and PhD degrees in environmental systems. His interests focus on environmental sensing and modeling of aquatic systems.